Analysis of radio-frequency absorption and electric and magnetic field enhancements due to surface roughness

Peng Zhang, Y. Y. Lau,[a] and R. M. Gilgenbach
Department of Nuclear Engineering and Radiological Sciences, University of Michigan, Ann Arbor, Michigan 48109-2104, USA

(Received 20 February 2009; accepted 14 April 2009; published online 4 June 2009)

The radio-frequency (rf) power absorption due to a small hemispherical protrusion on a resonant cavity's surface is computed analytically. This protrusion may assume arbitrary values of permittivity, permeability, and conductivity so that it may represent a foreign object. Under the assumption that the protrusion radius, a, is small compared with the rf wavelength, the power dissipated in the protrusion by the rf electric field and by the rf magnetic field are calculated explicitly. It is found that, in general, the heating by the rf magnetic field is dominant when $\delta/a < 1$, even for nonmagnetic materials, where δ is the skin depth associated with the protrusion material. The field enhancement factors for both the rf electric field and the rf magnetic field on the protrusion are also calculated analytically. They are found to decrease as δ/a increases. They are spot checked against the MAXWELL 3D code. These field enhancement factors are also consistent with the published results in the $\delta=0$ limit, in which case the protrusion may represent a small local bump on the surface of a superconducting cavity. © *2009 American Institute of Physics*. [DOI: 10.1063/1.3131844]

I. INTRODUCTION

Surface roughness may exert a profound effect in the performance of radio-frequency (rf) cavities or slow wave structures,[1–10] for example, in communication systems,[2,6,11,12] particle accelerators,[3,4,10,11,13,14] material characterization at microwave frequencies,[15,16] etc. Surface roughness may cause enhanced power absorption in these devices.[4,8–10,17–19] It may lead to excessive local electric field enhancement that triggers rf breakdown.[4,6,10,12,20–23] In a superconducting cavity, surface roughness may also cause local magnetic field enhancement that leads to abrupt quenching,[1,3,11] i.e., rapid loss of superconductivity.

Surface roughness may assume many forms. Small foreign objects might be attached to the cavity surface, and these impurities might have very different electrical properties from those of the presumably pristine metallic surface. Their presence is known to cause localized damage.[8,11,18] The metallic surface itself might not be perfectly smooth, in which case the roughness consists of the same material as the surface, i.e., no foreign materials are involved. Grain boundaries also make the surface microscopically rough.[19,24,25] Regardless of the origin of the roughness, of general interest is the additional rf power that would be absorbed due to the surface roughness, and the local enhancement in the rf electric field and in the rf magnetic field due to the change of the local geometry.

In this paper, we provide an accurate assessment of the additional heating, as well as the local rf electric field and rf magnetic field enhancements due to a small, local surface roughness. The crucial assumption is that this small roughness is hemispherical in shape, whose radius, a, is much less than $\lambda(a/\lambda \ll 1)$, where λ is the rf wavelength exterior to the protrusion. To isolate the effects of this roughness, we assume that it is setting on a perfectly conducting surface so that in the absence of this roughness, the rf electric field there, $\mathbf{E}_0$, is orthogonal to the surface; whereas the rf magnetic field there, $\mathbf{H}_0$, is tangential to the surface (Fig. 1). The relative magnitudes and the relative phases between $\mathbf{E}_0$ and $\mathbf{H}_0$ may be arbitrary so that this local roughness may be located anywhere on the surface of a conducting cavity or of a conducting waveguide. Another crucial assumption is that the hemispherical protrusion has a constant (complex) permittivity, $\varepsilon_1=\varepsilon_{r1}-j\sigma/\omega$, where σ is the electrical conductivity at the rf frequency ω, and a constant (real) permeability μ_1. While ε_{r1}, σ, and μ_1 are real constants, all assumed to be known, their values may be arbitrary. Thus, this roughness may represent a foreign object or it may be made of the same material as the conducting surface. The ratio δ/a may take on an arbitrary value ranging from zero to infinity, where $\delta=(2/\omega\mu_0\sigma)^{1/2}$ is the skin depth associated with protrusion

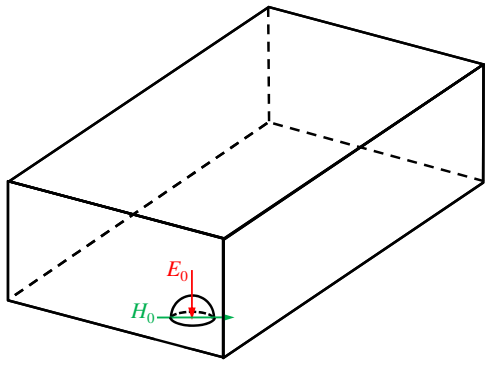

FIG. 1. (Color online) A small hemispherical bump on a conducting surface whose local rf electric field is $\mathbf{E}_0$ and local rf magnetic field is $\mathbf{H}_0$ in the absence of the bump.

[a]Electronic mail: yylau@umich.edu.

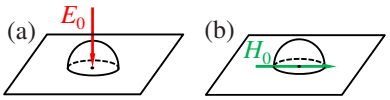

FIG. 2. (Color online) Decomposition of the local electromagnetic field $(\mathbf{E}_0,\mathbf{H}_0)$ into (a) the TE mode $(\mathbf{E}_0,0)$, and (b) the TM mode $(0,\mathbf{H}_0)$.

material, with $\delta\rightarrow\infty$ corresponding to an insulating protrusion and $\delta=0$ corresponding to a perfectly conducting protrusion.

In Sec. II, we transform the irregular geometry of a "hemispherical protrusion on a surface" (Fig. 1) into an equivalent, but highly symmetrical problem of a "spherical particulate in a spherical cavity" (Fig. 3 below) under the assumption that the radius a of the protrusion is much smaller than the wavelength (and also much smaller than the local radius of curvature of the surface if the cavity wall is not a flat surface). The perturbation by the small spherical particulate on the eigenfrequency of the spherical cavity then gives the rf power absorbed by the protrusion, as treated in Sec. III. The enhancement factors of the rf fields, as a result of the protrusion, are presented in Sec. IV. They are obtained from the perturbation on the eigenfunctions of the spherical cavity by the spherical particulate. Both rf electric field and rf magnetic field enhancement factors reduce to the established results in the appropriate limits. Section IV also presents spot checks of the field enhancement factors against the MAXWELL 3D code[26] results, adding plausibility of our approach. Concluding remarks are given in Sec. V.

Since the perturbations on the eigenmodes on the spherical cavity, by a small spherical particulate, were treated in some detail by Bosman *et al.*[27] and by Tang *et al.*,[28] we shall only quote their results when needed. Furthermore, Refs. 27 and 28 focused mainly on the rf heating of an isolated, freely suspended particulate. This paper extends their results to include the field enhancement factors in the rf electric field and rf magnetic field, and the resultant rf heating, for the important case where a small hemispherical particulate is attached to a perfect conductor.

II. THE MODEL

Despite the irregular geometry shown in Fig. 1 and the possibly strong coupling between the rf magnetic field and the rf electric field through the hemispherical protrusion, the problems of rf heating and of rf field enhancement at the protrusion can actually be solved *analytically* in the asymptotic limit $a/\lambda\ll 1$, without any restriction on the skin depth, δ. Our argument is as follows. In the *immediate neighborhood* of the protrusion (Fig. 1), the rf electromagnetic field, represented as $(\mathbf{E}_0,\mathbf{H}_0)$ when the protrusion is absent, may be considered as a linear combination of two modes: $(\mathbf{E}_0,0)$ and $(0,\mathbf{H}_0)$, each oscillating at the same frequency ω (Fig. 2). Because of the respective domination of the rf electric field and the rf magnetic field, we designate the $(\mathbf{E}_0,0)$ mode as the TE mode and the $(0,\mathbf{H}_0)$ as the TM mode. This mode designation, together with the corresponding ones in Fig. 3, follows Ref. 28. As we shall see, it also applies to incident transverse electromagnetic (TEM) plane wave in an open system with protrusions.

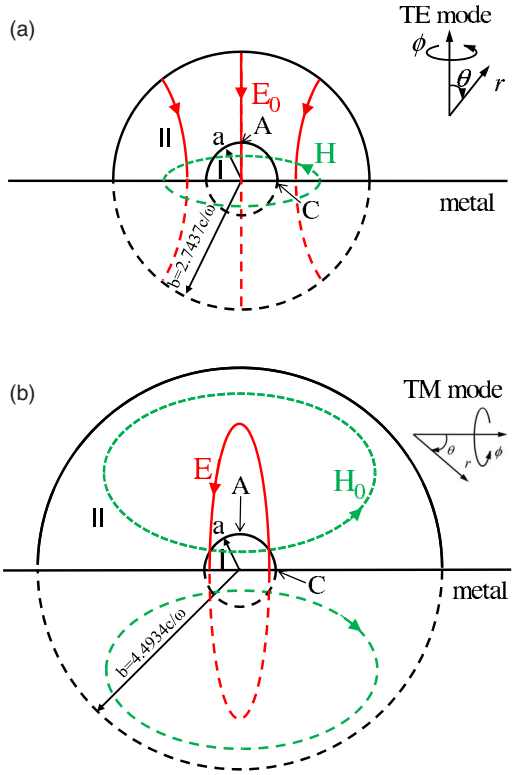

FIG. 3. (Color online) Transformation of the "protrusion on surface" problem into a spherical eigenmode problem for (a) the TE_{110} mode and (b) the TM_{110} mode. The mode index (110) refers to variations in r, θ, and φ. Note that by symmetry, the mode patterns in (a) or (b) are unchanged with or without a perfect conductor inserted in the horizontal midplane.

For the action of $(\mathbf{E}_0,0)$ on a small hemispherical protrusion [Fig. 2(a)], we now consider an auxiliary problem [Fig. 3(a)]. Figure 3(a) shows a perfectly conducting spherical cavity of radius b, whose natural frequency for the fundamental TE mode is ω when this cavity is empty (i.e., by setting $b=2.7437c/\omega$), and whose vacuum eigenmode at the center of cavity is $(\mathbf{E}_0,0)$. We now insert a spherical particulate of radius a and of the same permittivity $\varepsilon_1=\varepsilon_{r1}-j\sigma/\omega$, and the same permeability μ_1 at the center of this spherical cavity [Fig. 3(a)]. The high degree of spherical symmetry allows us to analytically calculate the perturbation on the eigenmode and the perturbation on the eigenfrequency by this spherical particulate.[27,28] The perturbation on the TE eigenmode gives the rf electric field enhancement factor, and the damping rate of the TE eigenmode gives the rf power dissipated in the lossy particulate.[27,28] These are also precisely the rf electric field enhancement for the small hemispherical protrusion on the flat plate [Fig. 2(a)] and the rf electric field energy that the (lossy) protrusion dissipated. This follows from symmetry of the fields: the rf electric field and the (vanishingly small) rf magnetic field in the spherical cavity, including the spherical particulate, are unchanged if we insert a horizontal, perfectly conducting plate that cuts the spherical cavity and spherical particulate in half [Fig. 3(a)]. In the immediate vicinity of the protrusion, the geometry, and rf field configuration also, between Figs. 2(a) and 3(a) are then equivalent in the asymptotic limit $a/\lambda\ll 1$. Since the perturbed TE eigenmode has been solved using the

full set of the Maxwell equations for Fig. 3(a), with the inclusion of the particulate, the calculation of the rf electromagnetic field for the TE mode is intrinsically self-consistent.[27,28]

Similarly, for the action of $(0,\mathbf{H}_0)$ on the hemispherical protrusion [Fig. 2(b)], we also consider the auxiliary problem [Fig. 3(b)], that of a perfectly conducting spherical cavity, whose natural frequency for the fundamental TM mode is also ω when the cavity is empty (i.e., by setting the cavity radius $b=4.4934c/\omega$), and whose vacuum eigenmode at the center of cavity is $(0,\mathbf{H}_0)$. We insert the same spherical particulate, of radius a and of the same permittivity $\varepsilon_1=\varepsilon_{r1}-j\sigma/\omega$, and the same permeability μ_1 at the center of this spherical cavity [Fig. 3(b)]. The perturbation on the TM eigenmode gives the rf magnetic field enhancement factor, and the damping rate of the TM eigenmode gives the rf power dissipated in the lossy particulate.[27,28] These are also precisely the rf magnetic field enhancement for the small hemispherical protrusion on the flat plate and the rf magnetic field energy that the (lossy) protrusion dissipated. This follows from symmetry of the fields: the rf magnetic field and the (vanishingly small) rf electric field in the spherical cavity, including the spherical particulate, are unchanged if we insert a horizontal, perfectly conducting plate that cuts the spherical cavity and spherical particulate in half [Fig. 3(b)]. In the immediate vicinity of the protrusion, the geometry, and rf field configuration also, between Figs. 2(b) and 3(b) are then equivalent in the asymptotic limit $a/\lambda \ll 1$. Since the perturbed TM eigenmode has been solved using the full set of the Maxwell equations, with the inclusion of the particulate, the calculation of the rf electromagnetic field for the TM mode is intrinsically self-consistent.

III. RF POWER ABSORPTION

The perturbation due to a small particulate located at the center of a perfectly conducting spherical cavity is studied by Bosman *et al.*[27] and Tang *et al.*[28] The particulate has radius a and the cavity has radius b. Hereafter, we follow Tang *et al.*[28] to use subscripts 1 and 2 to denote the values in region I $(r<a)$ and region II $(a<r<b)$ (Fig. 3). In these two regions, the permittivity is $\varepsilon_1=\varepsilon_{r1}-j\sigma/\omega$, and ε_2, respectively, and the permeability is μ_1 and μ_2 respectively, where ε_{r1}, σ, ε_2, μ_1, and μ_2 are all real and they may assume arbitrary values. Even though in this paper we will set $\varepsilon_2=\varepsilon_0$ and $\mu_2=\mu_0$, the formulas will be written for general values of ε_2 and μ_2 to conform with the notation of Ref. 28. In the absence of this particulate, the cavity admits the fundamental TE_{110} mode, which has a maximum rf electric field and a null rf magnetic field, at the center [Fig. 3(a)], as well as the TM_{110} mode, which has a maximum rf magnetic field, and a null rf electric field, at the center [Fig. 3(b)]. In the empty cavity, both the TE mode and TM mode have an infinite quality factor Q since the cavity wall is lossless. The eigenfrequencies ω_E and ω_M (both equal to ω) for the TE_{110} and TM_{110} modes are given by $\eta_E=2.743\,71$ and $\eta_M=4.4934$, respectively, with $\eta_{E,M}=\omega_{E,M}b(\varepsilon_2\mu_2)^{1/2}=2\pi b/\lambda$.[29] When a small, lossy particulate is introduced at the center of the cavity, the modes would be slightly damped, the eigenmode frequency becomes complex, and the quality factor Q becomes finite. The change of Q in the TE (TM) mode gives the power dissipation due to this lossy particulate by the rf electric (magnetic) field. The change in the eigenfrequencies, $\delta\omega$, due to the particulate reads

$$\frac{\delta\omega}{\omega_E}=\frac{\delta\eta}{\eta_E}\approx\frac{Y'(\eta_E)}{\eta_E J''(\eta_E)}\left[\frac{J(\xi_{2E})}{Y(\xi_{2E})}\right]\times\left[\frac{Z_1A(\xi_{1E})-A(\xi_{2E})}{Z_1A(\xi_{1E})-B(\xi_{2E})}\right]\quad\text{(TE mode)},\tag{1}$$

$$\frac{\delta\omega}{\omega_M}=\frac{\delta\eta}{\eta_M}\approx\frac{y(\eta_M)}{\eta_M j'(\eta_M)}\left[\frac{J'(\xi_{2M})}{Y'(\xi_{2M})}\right]\times\left[\frac{Z_1/A(\xi_{1M})-1/A(\xi_{2M})}{Z_1/A(\xi_{1M})-1/B(\xi_{2M})}\right]\quad\text{(TM mode)},\tag{2}$$

for the TE and TM modes, respectively [cf. Eqs. (15) and (28) of Ref. 28], where

$$j(\xi)=\frac{\sin\xi}{\xi^2}-\frac{\cos\xi}{\xi},\tag{3}$$

$$y(\xi)=-\frac{\cos\xi}{\xi^2}-\frac{\sin\xi}{\xi},\tag{4}$$

$$J(\xi)=\xi j(\xi),\quad Y(\xi)=\xi y(\xi),\tag{5}$$

$$A(\xi)=\frac{J'(\xi)}{J(\xi)},\quad B(\xi)=\frac{Y'(\xi)}{Y(\xi)},\tag{6}$$

$$Z_1=\frac{\sqrt{\mu_1/\mu_2}}{\sqrt{\varepsilon_1/\varepsilon_2}},\tag{7}$$

and the prime denotes the derivative with respect to the argument. In the arguments, $\xi_{2E}=\eta_E(a/b)$ and $\xi_{2M}=\eta_M(a/b)$ are both real, $\xi_{1E}=\omega_E(\varepsilon_1\mu_1)^{1/2}a$, $\xi_{1M}=\omega_M(\varepsilon_1\mu_1)^{1/2}a$, in which μ_1 (permeability of region I) is real, $\varepsilon_1=\varepsilon_{1r}-j\sigma/\omega$ (permittivity of region I) is complex. Once more, Eqs. (1) and (2) are valid as long as $a/\lambda\ll 1$, regardless of the values of ε_{r1}, σ, ε_2, μ_1, and μ_2.

The real parts of Eqs. (1) and (2) give the detune of the eigenmode frequency and the imaginary parts give the damping rate $\gamma_{E,M}$, which is related to the average power loss P and the quality factor Q through the relationship (Ref. 29),

$$P=2\gamma U=\omega U/Q,\tag{8}$$

where U is the average electromagnetic energy stored in the eigenmode of the empty cavity. The power dissipations for the TE and TM modes for Fig. 2, denoted by P_E and P_M, respectively, then read

$$P_E=\alpha_E\omega_E\left(\frac{1}{2}\varepsilon_2E_0^2\right)V_a,\tag{9a}$$

$$\alpha_E=0.041\,31\left(\frac{\lambda}{a}\right)^3\frac{\gamma_E}{\omega_E},\tag{9b}$$

$$P_M = \alpha_H \omega_M \left(\frac{1}{2}\mu_2 H_0^2\right) V_a, \tag{10a}$$

$$\alpha_H = 0.077\ 67 \left(\frac{\lambda}{a}\right)^3 \frac{\gamma_M}{\omega_M}, \tag{10b}$$

where $E_0(H_0)$ is the peak value of the rf electric (magnetic) field of the TE (TM) mode at the center of the cavity in the absence of the spherical particulate (Fig. 3), whose half volume is $V_a=(2\pi/3)a^3$, and $\alpha_E(\alpha_H)$ is known as the particulate polarizability[30–32] for the TE (TM) mode [cf. Eqs. (20) and (32) of Ref. 28].

The asymptotic formulas for α_E in Eq. (9b) and α_H in Eq. (10b) may be expressed in terms of the skin depth $\delta=(2/\omega\mu_2\sigma)^{1/2}$ [cf. Eqs. (36) and (37) of Ref. 28],

$$\alpha_E \cong 9\pi^2 \left(\frac{a\delta}{\lambda^2}\right)\sqrt{\frac{\mu_1}{\mu_2}}, \quad \sqrt{\frac{\mu_2}{\mu_1}}\frac{\delta}{a} \ll 1, \tag{11a}$$

$$\alpha_E \cong 18\pi^2(\delta/\lambda)^2,$$

$$1 \ll \sqrt{\frac{\mu_2}{\mu_1}}\frac{\delta}{a} \ll \frac{1}{\pi\sqrt{2}}\sqrt{\frac{\varepsilon_2}{\varepsilon_{1r}}}\sqrt{\frac{\mu_2}{\mu_1}}\left(\frac{\lambda}{a}\right), \tag{11b}$$

$$\alpha_E \cong \frac{(\lambda/\delta)^2}{2\pi^2}\left(\frac{3}{2+\varepsilon_{1r}/\varepsilon_2}\right)^2,$$

$$1 \ll \frac{1}{\pi\sqrt{2}}\sqrt{\frac{\varepsilon_2}{\varepsilon_{1r}}}\sqrt{\frac{\mu_2}{\mu_1}}\left(\frac{\lambda}{a}\right) \ll \sqrt{\frac{\mu_2}{\mu_1}}\frac{\delta}{a}, \tag{11c}$$

$$\alpha_H \cong \frac{9}{4}\frac{\delta}{a}\sqrt{\frac{\mu_1}{\mu_2}}, \quad \sqrt{\frac{\mu_2}{\mu_1}}\frac{\delta}{a} \ll 1, \tag{12a}$$

$$\alpha_H \cong \frac{1}{5}\left(\frac{a}{\delta}\right)^2\left(\frac{\mu_1}{\mu_2}\right)^2\left(\frac{3}{2+\mu_1/\mu_2}\right)^2, \quad \sqrt{\frac{\mu_2}{\mu_1}}\frac{\delta}{a} \gg 1. \tag{12b}$$

Tang *et al.*[28] shows that the asymptotic formulas, Eqs. (11a)–(11c), (12a), and (12b), give an excellent qualitative representation of the exact forms, Eqs. (9b) and (10b). Figure 4(a) shows the asymptotes of α_E as a function of δ/a for different values of λ/a, for the special case $\mu_1=\mu_2=\mu_0$, and $\varepsilon_{1r}=\varepsilon_2=\varepsilon_0$. From the interception of the asymptotic expansions (11b) and (11c), one estimates that the maximum value of α_E is of order 3, occurring at a value of $\delta/a=0.13(\lambda/a)$, as shown in Fig. 4(a). Figure 4(b) shows the asymptotes of α_H as a function of δ/a for the same special case $\mu_1=\mu_2=\mu_0$, and $\varepsilon_{1r}=\varepsilon_2=\varepsilon_0$. Note from Eqs. (12a) and (12b) that these asymptotes are independent of λ/a for $\lambda/a \gg 1$. The maximum value of α_H is about 1.0, occurring at a value of $\delta/a=0.446$ approximately, as shown in Fig. 4(b). Taking the ratio of Eq. (11a) and (12a), one obtains $\alpha_H/\alpha_E=(\lambda/2\pi a)^2 \gg 1$ for a good conducting particulate ($\delta/a \ll 1$), as is also evident in Fig. 4. Thus, heating by the rf magnetic field dominates over the heating by the rf electric field when $\delta/a<1$.[8,27,28,33] We should emphasize that, physically, "heating by the rf magnetic field" is actually the same as *Ohmic heating* due to the rf *electric* field that is *induced* within the particulate/protrusion by the external rf magnetic field component, and this is the physical basis of derivation of the magnetic polarizability for nonmagnetic materials by Landau and Lifshitz.[32] Using Eqs. (11) and (12), Eqs. (9) and (10) yield

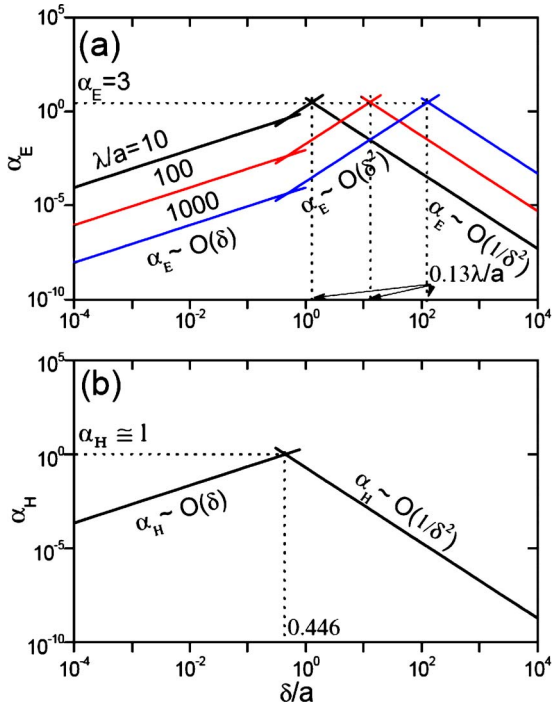

FIG. 4. (Color online) The asymptotes for (a) α_E and (b) α_H as a function of δ/a for $\mu_1/\mu_2=1$, $\varepsilon_{1r}/\varepsilon_2=1$ and various values of λ/a. These asymptotes yield approximate maximum values of $\alpha_E=3$ and $\alpha_H=1.0$. Note that the scaling law for α_H is independent of λ/a for $\lambda/a \gg 1$.

$$P_E = \begin{cases} 9\pi^2 \dfrac{a\delta}{\lambda^2}\omega U_E V_a, & \dfrac{\delta}{a} \ll 1, \\ 18\pi^2\left(\dfrac{\delta}{\lambda}\right)^2 \omega U_E V_a, & 1 \ll \dfrac{\delta}{a} \ll \dfrac{\lambda}{a}, \\ \dfrac{1}{2\pi^2}\left(\dfrac{\lambda}{\delta}\right)^2 \omega U_E V_a, & 1 \ll \dfrac{\lambda}{a} \ll \dfrac{\delta}{a}, \end{cases} \tag{13}$$

$$P_M = \begin{cases} \dfrac{9}{4}\left(\dfrac{\delta}{a}\right)\omega U_H V_a, & \dfrac{\delta}{a} \ll 1, \\ \dfrac{1}{5}\left(\dfrac{a}{\delta}\right)^2 \omega U_H V_a, & \dfrac{\delta}{a} \gg 1, \end{cases} \tag{14}$$

where $U_E=(1/2)\varepsilon_0 E_0^2$ and $U_H=(1/2)\mu_0 H_0^2$ for the special case $\mu_1=\mu_2=\mu_0$ and $\varepsilon_{1r}=\varepsilon_2=\varepsilon_0$.

To quantify the additional heating due to surface roughness relative to the intrinsic Ohmic loss in the flat surface, let us now assume that the flat surface is slightly lossy, characterized by its skin depth δ_s. To get an idea on the order of magnitude, let us consider a planar, TEM wave that propagates on the flat surface whose electric and magnetic field amplitude satisfies $E_0=(\mu_0/\varepsilon_0)^{1/2}H_0$ (Fig. 2). Over an area of 1 m^2 on this surface, the Ohmic power loss on this flat surface is readily shown to be $P_{\text{flat}}=\pi(\delta_s/\lambda)S$, where $S=(1/2)E_0H_0=(1/2)E_0^2(\varepsilon_0/\mu_0)^{1/2}$ is the Poynting flux [cf. Eq. (5) on p. 157 of Ramo *et al.*, Ref. 29]. Over this unit surface area, let there be N hemispherical protrusions of radius a so

that the fraction of the surface area that is bumpy is $f_{\text{bump}} = N\pi a^2$. These protrusions may be considered independent if their average separation is much larger than a.[28] If each protrusion consumes an additional rf power $(P_E + P_M)$, where P_E and P_M are given by Eqs. (9a) and (10a), then we obtain

$$R = \frac{P_{\text{protusions}}}{P_{\text{flat}}} = \frac{N(P_E + P_M)}{\pi(\delta_s/\lambda)(E_0^2/2)\sqrt{\varepsilon_0/\mu_0}}, \tag{15}$$

which is the ratio of the additional rf power dissipated by the surface roughness to the intrinsic Ohmic loss on the pristine flat surface. The three following cases are next examined to illustrate its order of magnitude.

(A) If the hemispherical protrusions are made of the same conducting materials as the flat surface, we set $\delta = \delta_s$ in Eq. (14) and ignore P_E in comparison with P_M (assuming $\delta < a$) to obtain

$$R = 3f_{\text{bump}}, \tag{16}$$

where f_{bump} is the fraction of the surface area covered by roughness. Thus, for a nominally flat superconducting surface, where f_{bump} is expected to be very small, the additional Ohmic heating on the rough surface as measured by R (in the absence of foreign contaminants) is unlikely to be the reason for any loss of superconductivity. On the other hand, on an ordinary conductor, if its surface exhibits excessive rf power loss, the likely culprit would be foreign objects or grain boundaries that introduce significant additional surface resistance.

(B) If the protrusions are made of foreign objects, the maximum amount of their Ohmic loss through the rf electric field may be estimated by inserting the approximate maximum value of $\alpha_E = 3$ into Eq. (9a); see Fig. 4(a). Equation (15) then gives, upon ignoring the P_M term,

$$R = R_{\max}(\text{TE}) = \left(\frac{4a}{\delta_s}\right) f_{\text{bump}}. \tag{17}$$

(C) Likewise, if the protrusions are made of foreign objects, the maximum amount of their Ohmic loss through the rf magnetic field may be estimated by inserting the approximate maximum value of $\alpha_H = 1.0$ into Eq. (10a); see Fig. 4(b). Equation (15) then gives, upon ignoring the P_E term,

$$R = R_{\max}(\text{TM}) = \left(\frac{1.33a}{\delta_s}\right) f_{\text{bump}}. \tag{18}$$

Equation (15) may provide a useful estimate on the additional loss due to surface features that are difficult to simulate directly in a numerical code. If Ohmic loss is a serious issue, as expected in a submillimeter traveling wave tube because of its low gain,[2] additional loss due to surface roughness poses a very serious threat. Equation (15), together with experimental measurements of the geometric surface features, may provide a characterization of such additional loss, and the latter may then be included in a more realistic design.

IV. RF FIELD ENHANCEMENTS

The modifications of the eigenfunctions by the spherical particulate in Figs. 3(a) and 3(b) give the enhancements in the rf electric field and in the rf magnetic field for the hemispherical protrusions in Figs. 2(a) and 2(b), respectively. We treat these two cases separately below. They were not examined in Refs. 27 and 28.

A. rf electric field enhancement

The local rf electric field at the location of the protrusion in Fig. 3(a) may be obtained from the r-component and θ-component of electric field in region II for the TE mode. They read [cf. Eq. (9) of Ref. 28]

$$E_r = \frac{2B\cos\theta}{j\omega\varepsilon_2 r}[Y'(\eta)j(k_2 r) - J'(\eta)y(k_2 r)], \tag{19}$$

$$E_\theta = \frac{B\sin\theta}{j\omega\varepsilon_2 r}[Y'(\eta)J'(k_2 r) - J'(\eta)Y'(k_2 r)], \tag{20}$$

where B is an arbitrary constant, $j(\xi)$, $y(\xi)$, $J(\xi)$, and $Y(\xi)$ are defined in Eqs. (3)–(5), $k_2 = \omega(\varepsilon_2\mu_2)^{1/2}$, $\eta = k_2 b$, and the prime denotes the derivative with respect to the argument. For these fields to give a constant rf electric field E_0, at the center of the cavity in the absence of the particulate, we find the constant B to be related to E_0 by

$$E_0 = B\left(-j\frac{2}{3}Y'(\eta_E)\right)\sqrt{\frac{\mu_2}{\varepsilon_2}}, \tag{21}$$

where $\eta_E = 2\pi b/\lambda = 2.743\,71$.

The introduction of a small protrusion modifies the eigenvalue by a small amount, $\omega = \omega_E + \delta\omega$, $\eta = \eta_E + \delta\eta$, and $\xi_2 = \xi_{2E} + \delta\xi_2$, where $\xi_{2E} = 2\pi a/\lambda = \eta_E(a/b)$. It can be easily shown that $\delta\omega/\omega_E = \delta\eta/\eta_E = \delta\xi_2/\xi_{2E}$, given by Eq. (1). By evaluating Eqs. (19) and (20) at point A, the apex, and at point C, the base, respectively [Fig. 3(a)], and expanding about the unperturbed values η_E, ω_E, and ξ_E, we obtain the amplitude of the electric field at point A and C in the limit $a/\lambda \ll 1$,

$$E_A = \beta_{EA}E_0, \tag{22a}$$

$$\beta_{EA} = \left|1 + \frac{\delta\omega}{\omega_E}F_A\right|, \tag{22b}$$

$$F_A = -1 + \eta_E\frac{Y''(\eta_E)}{Y'(\eta_E)} + \xi_{2E}\frac{j'(\xi_{2E})}{j(\xi_{2E})} - \eta_E\frac{J''(\eta_E)y(\xi_{2E})}{Y'(\eta_E)j(\xi_{2E})}, \tag{22c}$$

$$E_C = \beta_{EC}E_0, \tag{23a}$$

$$\beta_{EC} = \left|1 + \frac{\delta\omega}{\omega_E}F_C\right|, \tag{23b}$$

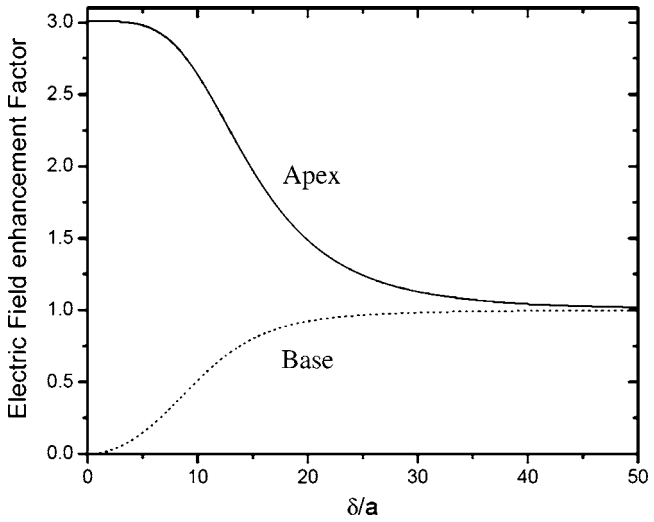

FIG. 5. The electric field enhancement factor on the hemispherical protrusion at the apex (β_{EA}, solid curve) and at the base (β_{EC}, dotted curve) as a function of δ/a, setting $\mu_1/\mu_2=1$, $\varepsilon_{1r}/\varepsilon_2=1$, and $\lambda/a=100$.

$$F_C = -1 + \eta_E \frac{Y''(\eta_E)}{Y'(\eta_E)} + \xi_{2E} \frac{J''(\xi_{2E})}{J'(\xi_{2E})} - \eta_E \frac{J''(\eta_E)Y'(\xi_{2E})}{Y'(\eta_E)J'(\xi_{2E})}, \quad (23c)$$

where β_{EA} and β_{EC} are the electric field enhancement factor at point A and C due to the presence of the hemispherical protrusion at the flat surface, respectively, and $\delta\omega/\omega_E$ is given by Eq. (1).

Figure 5 shows β_{EA} and β_{EC} as a function of δ/a, setting $\mu_1/\mu_2=1$, $\varepsilon_{1r}/\varepsilon_2=1$, and $\lambda/a=100$. As the skin depth becomes much smaller than the radius of the bump, $\delta/a\sim 0$, the bump is nearly perfect conducting, the field enhancement factor at apex is around 3, which agrees well with previous studies.[34,35] At the base point C, the electric field is forced to become normal to both the hemispherical surface and the flat surface, which are perpendicular to each other [Fig. 3(a)], thus the electric field vanishes and the electric field enhancement factor approaches zero. On the other hand, as the skin depth assumes a very large value, the bump is almost dielectric, with the same permeability and permittivity as vacuum, $\mu_1/\mu_2=1$, $\varepsilon/\varepsilon_2\cong\varepsilon_{1r}/\varepsilon_2=1$, the rf electric field is not perturbed and the field enhancement factor at both points A and C converges to the value of 1, as expected, and shown also in Fig. 5.

A three-dimensional finite element code MAXWELL 3D (Ref. 26) was used to verify the field enhancement factor calculated analytically as well as the field distribution. The hemispherical protrusion was situated on a flat, perfectly conducting surface, as shown in Fig. 6. The electric field is strongest at the apex and weakest at the base. In Fig. 6(a), by reading the color bar, the electric field at the apex is roughly three times of the background value, which is confirmed in Fig. 6(b), where the magnitude of electric field, $(E_r^2+E_\theta^2)^{1/2}$, is plotted along a horizontal line at a distance of one protrusion radius above the flat surface, showing a field enhancement factor of 3 clearly. As shown in Fig. 6(b), the analytical calculation from Eqs. (19) and (20) gives identical results as the simulation. Note that the field enhancement profile is independent of the radius of the protrusion.

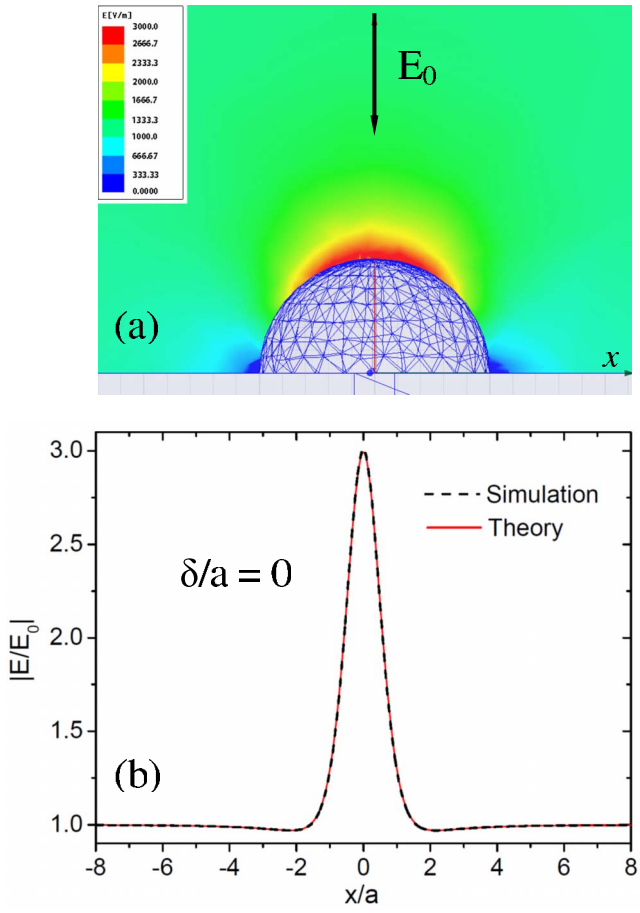

FIG. 6. (Color online) MAXWELL 3D results of (a) electric field distribution around the hemispherical bump, (b) magnitude of electric field along a horizontal line 0.5 cm (bump radius) above the flat surface (dashed line), which agrees extremely well with the analytical calculation (solid line). E_0 is the electric field far away from the bump.

B. rf magnetic field enhancement

The local magnetic field at the location of the bump on a flat surface can be similarly calculated using the model of Fig. 3(b). The θ-component and r-component of the rf magnetic field in region II of Fig. 3(b) are [cf. Eq. (25) of Ref. 28],

$$H_\theta = \frac{D\sin\theta}{j\omega\mu_2 r}[y(\eta)J'(k_2 r) - j(\eta)Y'(k_2 r)], \quad (24)$$

$$H_r = \frac{2D\cos\theta}{j\omega\mu_2 r}[y(\eta)j(k_2 r) - j(\eta)y(k_2 r)], \quad (25)$$

respectively, where D is an arbitrary constant, $j(\xi)$, $y(\xi)$, $J(\xi)$, and $Y(\xi)$ are defined in Eqs. (3)–(5), $k_2=\omega(\varepsilon_2\mu_2)^{1/2}$, $\eta=k_2 b$, and the prime denotes the derivative with respect to the argument. For these fields to give a constant rf magnetic field H_0, at the center of the cavity in the absence of the particulate, the constant D is related to H_0 by

$$H_0 = D\left(-j\frac{2}{3}y(\eta_M)\right)\sqrt{\frac{\varepsilon_2}{\mu_2}}, \quad (26)$$

where $\eta_M=2\pi b/\lambda=4.4934$.

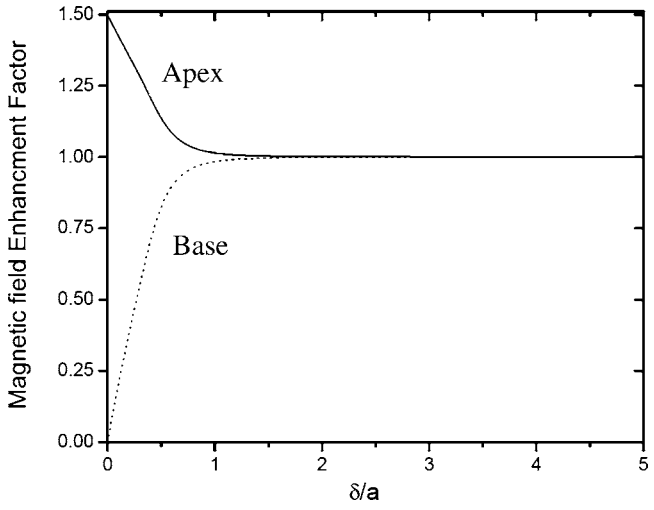

FIG. 7. The magnetic field enhancement factor on the hemispherical protrusion at the apex point A (β_{MA}, solid curve) and at the base point C (β_{MC}, dotted curve) as a function of δ/a, setting $\mu_1/\mu_2=1$, $\varepsilon_{1r}/\varepsilon_2=1$, and $\lambda/a=100$.

The introduction of a small protrusion modifies the eigenvalue η_M by a small amount. Analogous to Eqs. (22) and (23), we obtain the amplitude of the rf magnetic field at points A and C of Fig. 3(b) in the limit $a/\lambda \ll 1$,

$$H_A = \beta_{MA} H_0, \tag{27a}$$

$$\beta_{MA} = \left| 1 + \frac{\delta\omega}{\omega_M} G_A \right|, \tag{27b}$$

$$G_A = -1 + \eta_M \frac{y'(\eta_M)}{y(\eta_M)} + \xi_{2M} \frac{J''(\xi_{2M})}{J'(\xi_{2M})} - \eta_M \frac{j'(\eta_M) Y'(\xi_{2M})}{y(\eta_M) J'(\xi_{2M})}, \tag{27c}$$

$$H_C = \beta_{MC} H_0, \tag{28a}$$

$$\beta_{MC} = \left| 1 + \frac{\delta\omega}{\omega_M} G_C \right|, \tag{28b}$$

$$G_C = -1 + \eta_M \frac{y'(\eta_M)}{y(\eta_M)} + \xi_{2M} \frac{j'(\xi_{2M})}{j(\xi_{2M})} - \eta_M \frac{j'(\eta_M) y(\xi_{2M})}{y(\eta_M) j(\xi_{2M})}, \tag{28c}$$

where β_{MA} and β_{MC} are the magnetic field enhancement factor at point A and C due to the presence of the hemispherical protrusion at the flat surface, respectively, $\xi_{2M}=2\pi a/\lambda = \eta_M(a/b)$ and $\delta\omega/\omega_M$ is given by Eq. (2).

Figure 7 shows β_{MA} and β_{MC} as a function of δ/a, setting $\mu_1/\mu_2=1$, $\varepsilon_{1r}/\varepsilon_2=1$ and $\lambda/a=100$. As the skin depth becomes much smaller than the radius of the bump, $\delta/a \sim 0$, the bump is nearly perfectly conducting, the magnetic field enhancement factor at apex is 1.5, which confirms the result obtained by Shemelin and Padamsee,[1] who simulated the magnetic field enhancement at bumps on the surface of a pill-box cavity using the code SLANS2. Note that this magnetic field enhancement factor at the apex of a hemispherical bump on a flat surface is the same as that of an isolated perfectly conducting sphere inserted in a uniform magnetic field.[36] Note from Fig. 7 that the maximum magnetic field enhancement factor is given by materials with zero skin depth, i.e., a superconductor, in which case the local high magnetic field could exceed the critical magnetic field for superconductivity, even though the rf magnetic field is below this critical value for a pristine, flat surface. Thus surface roughness could lead to abrupt loss of superconductivity.[1,11] Note further that this magnetic field enhancement factor is independent of the size of the hemispherical protrusion. Thus, it is extremely important to create ultrasmooth, polished surfaces to retain superconductivity in the presence of large rf magnetic fields, and this is consistent with the current challenge in superconducting cavity fabrication. At the base point C, the magnetic field normal to the bump surface vanishes and the field enhancement factor becomes 0. When the skin depth becomes comparable to the bump radius, the magnetic field enhancement factor at both point A and C becomes nearly unity (Fig. 7).

The MAXWELL 3D code[26] was used again to verify the magnetic field enhancement factor calculated analytically as well as the field distribution due to the hemispherical protrusion situated on a perfectly conducting surface, as shown in Fig. 8. The magnetic field is strongest along the great circle whose plane is perpendicular to the applied magnetic field, according to color bar in Fig. 8(a). The magnetic field at the apex is roughly 1.5 times of the background value. The magnitude of the magnetic field, $(H_r^2+H_\theta^2)^{1/2}$, is plotted along two horizontal lines at a distance of one bump radius above the flat surface, one line (line 1) in the plane parallel to and the other line (line 2) perpendicular to the applied magnetic field, as shown in Figs. 8(b) and 8(c), respectively. Both plots clearly show a magnetic field enhancement of 1.5. The simulation results agreed extremely well with our analytically calculated results from Eq. (24) and (25), as shown by the solid lines in Figs. 8(b) and 8(c). The field enhancement profile is independent of the size of the protrusion.

V. CONCLUDING REMARKS

This paper gives a self-consistent, accurate evaluation of the modification of the electromagnetic field due to a hemispherical protrusion setting on a locally flat conducting surface. Two major assumptions were made: (a) The size of the protrusion is small compared with the wavelength of the radiation, and with the local radius of curvature if the surface is curved, and (b) the complex permittivity and permeability of the protrusion are constant. The latter constants may assume arbitrary values however. The local rf electric and rf magnetic fields, $\mathbf{E}_0$ and $\mathbf{H}_0$ in the absence of the protrusion, may have arbitrary magnitudes and phases between them. The Ohmic absorption by the protrusion is calculated, and compared with the intrinsic Ohmic absorption of an otherwise flat surface. Our study suggests that if excessive Ohmic loss on a nominally flat metallic surface occurs, it is most likely due to foreign objects or grain boundaries that greatly increase the surface resistance.

The rf electric field enhancement and rf magnetic field

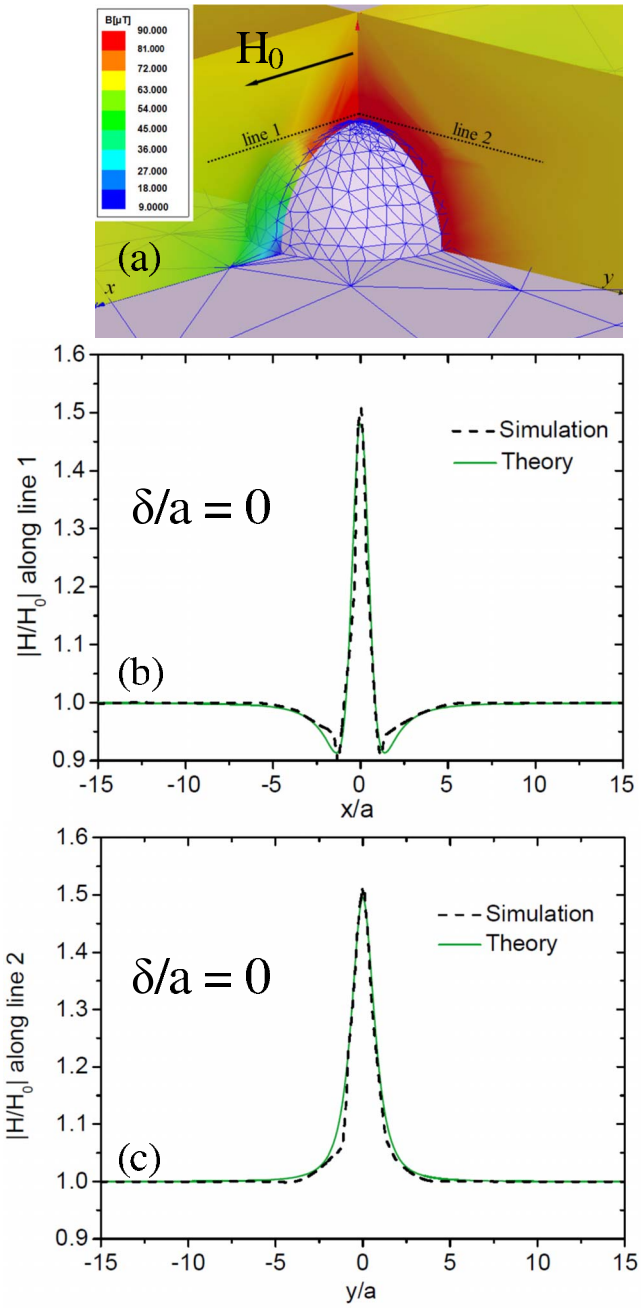

FIG. 8. (Color online) MAXWELL 3D results. (a) Magnetic field distribution around the hemispherical bump in the plane parallel and perpendicular to the applied field. Plot of the magnitude of magnetic field (dashed lines) along line 1 (b), and along line 2 (c), both are horizontal lines 1.0 cm (one bump radius) above the flat surface. Also shown are the analytical calculations (solid lines). H_0 is the magnetic field far away from the bump.

enhancement due to the hemispherical protrusion is also calculated. These field enhancement factors do not depend on the size of the protrusion, and they are modest (maximum value of 3 for rf electric field enhancement and 1.5 for rf magnetic field enhancement). While these are only modest enhancements and are simply the classical, static value expected on a conducting protrusion, the magnetic field enhancement due to surface roughness has been a major concern in the design of superconducting cavities. It is interesting to note that in all of our calculations of the perturbed electromagnetic fields, we assume a small protrusion. Yet the above-quoted finite values of field enhancement factors remain as long as the protrusion exists, regardless of its size. That is, a regular perturbation technique yields a finite but different result in the limit of the vanishingly small expansion parameter (a/λ). The approach of decomposition into separate TE and TM modes, and the perturbation techniques in the smallness of the protrusion radius, apparently are valid, as our results agree with numerical codes, and with the known results in the appropriate limit in this purely classical (non-quantum-mechanical) analysis.

Since the amplitudes and the phases of $\mathbf{E}_0$ and $\mathbf{H}_0$ of the local electromagnetic field are arbitrary, this electromagnetic field may be due to an incident wave at arbitrary incident angle and arbitrary polarization. Since we have self-consistently and accurately calculated the (nontrivial) modification of $\mathbf{E}_0$ and $\mathbf{H}_0$ by a local hemispherical protrusion, we have essentially paved the way to calculate the scattered radiation of an arbitrary incident wave due to such a protrusion, subject only to the two relatively weak assumptions stated in the first paragraph of this section.

Finally, what we have calculated here includes the complete rf field solutions at a triple point, defined as the interface between dielectric, metal, and vacuum.[37,38] The maximum field enhancement factors are given by that of a perfect conductor, in the limit of a static field (electric or magnetic). Thus, if we are only interested in the maximum field enhancement factors for a complex protrusion geometry, we may simply use electrostatic and magnetostatic field solvers for that geometry.[1,20,21,34–36] However, the rf heating in such a protrusion is considerably more difficult to assess.

ACKNOWLEDGMENTS

This work was supported by AFOSR Cathode and Breakdown MURI04 Grant No FA9550-04-1-0369, and by AFRL, AFOSR, L-3 Communications and Northrop-Grumman Corporation.

[1]V. Shemelin and H. Padamsee, SRF 080903–04, TESLA, 2008.
[2]J. H. Booske, Phys. Plasmas **15**, 055502 (2008).
[3]Y. Iwashita and Y. Tajima, Phys. Rev. ST Accel. Beams **11**, 093501 (2008); Y. Iwashita and T. Higo, Proceedings of the LINAC, 2004 (unpublished).
[4]M. Petelin, J. Hirshfield, Y. Y. Danilov, S. Kuzikov, V. Pavelyev, D. Schegolkov, and A. Yunakovsky, AIP Conf. Proc. **807**, 408 (2006).
[5]G. P. Scheitrum, in *Modern Microwave and Millimeter-Wave Power Electronics*, edited by R. J. Barker, J. H. Booske, N. C. Luhmann, Jr., and G. S. Nusinovich (IEEE, Piscataway, 2005), Chap. 7, p. 343.
[6]V. I. V. Bobkov, J.-M. Noterdaeme, and R. Wilhelm, Surf. Coat. Technol. **200**, 822 (2005).
[7]H. Pandit, D. Shi, N. H. Babu, X. Chaud, D. A. Cardwell, P. He, D. Isfort, R. Tournier, D. Mast, and A. M. Ferendeci, Physica C **425**, 44 (2005).
[8]V. A. Dolgashev and S. G. Tantawi, AIP Conf. Proc. **691**, 151 (2003).
[9]D. P. Pritzkau and R. H. Siemann, Phys. Rev. ST Accel. Beams **5**, 112002 (2002); D. P. Pritzkau, "RF pulse heating," Ph.D. thesis, Stanford University, 2001.
[10]W. Wuensch, AIP Conf. Proc. **647**, 506 (2002).
[11]H. Padamsee, Supercond. Sci. Technol. **14**, R28 (2001); H. Padamsee, J. Knobloch, and T. Hays, *RF Superconductivity for Accelerators* (Wiley, New York, 1998).
[12]J. B. O. Caughman, C. Castano-Giraldo, M. Aghazarian, F. W. Baity, D. A. Rasmussen, and D. N. Ruzic, AIP Conf. Proc. **933**, 195 (2007).
[13]E. W. Collings, M. D. Sumption, and T. Tajima, Supercond. Sci. Technol. **17**, S595 (2004).
[14]J. J. Song, S. Bajikar, Y. W. Kang, R. L. Kustom, D. C. Mancini, A.

Nassiri, and B. Lai, Proceedings of the IEEE PAC97, Vancouver, 1997 (unpublished), p. 461.
[15]M. J. Lancaster, *Passive Microwave Device Applications of High-Temperature Superconductors* (Cambridge University Press, Cambridge, 1997).
[16]Z. Zhai, C. Kusko, N. Hakim, and S. Sridhar, Rev. Sci. Instrum. **71**, 3151 (2000).
[17]L. K. Ang, Y. Y. Lau, R. M. Gilgenbach, and H. L. Spindler, Appl. Phys. Lett. **70**, 696 (1997).
[18]H. Bosman, Ph.D. thesis, University of Michigan, 2004.
[19]T. Sun, B. Yao, A. P. Warren, K. Barmak, M. F. Toney, R. E. Peale, and K. R. Coffey, Phys. Rev. B **79**, 041402(R) (2009).
[20]R. Miller, Y. Y. Lau, and J. H. Booske, Appl. Phys. Lett. **91**, 074105 (2007).
[21]K. L. Jensen, Y. Y. Lau, D. W. Feldman, and P. G. O'Shea, Phys. Rev. ST Accel. Beams **11**, 081001 (2008).
[22]P. Wilson, High Gradient Workshop, 2007 (unpublished).
[23]T. A. de Assis, F. Borondo, R. M. Benito, and R. F. S. Andrade, Phys. Rev. B **78**, 235427 (2008).
[24]A. A. Neuber, L. Laurent, Y. Y. Lau, and H. Krompholz, in *High-Power Microwave Sources and Technologies*, edited by R. J. Barker and E. Schamiloglu (IEEE, New York, 2001), Chap. 10, p. 325.
[25]J. Knobloch, R. L. Geng, M. Liepe, and H. Padamsee, Proceedings of the SRF, Santa Fe, NM, 1999 (unpublished).
[26]http://www.ansoft.com
[27]H. Bosman, W. Tang, Y. Y. Lau, and R. M. Gilgenbach, Appl. Phys. Lett. **85**, 3319 (2004).
[28]W. Tang, H. Bosman, Y. Y. Lau, and R. M. Gilgenbach, J. Appl. Phys. **97**, 114915 (2005).
[29]S. Ramo, J. R. Whinnery, and T. Van Duzer, *Fields and Waves in Communications Electronics* (Wiley, New York, 1994), p. 508.
[30]G. L. Carr, S. Perkowitz, and D. B. Tanner, in *Infrared and MM Waves*, edited by K. J. Button (Academic, New York, 1985), Vol. 13, p. 171.
[31]R. E. Collin, *Field Theory of Guided Waves*, 2nd ed. (IEEE, New York, 1990).
[32]L. D. Landau and E. M. Lifshitz, *Electrodynamics of Continuous Media* (Pergamon, New York, 1984), p. 322.
[33]J. Cheng, R. Roy, and D. Agrawal, J. Mater. Sci. Lett. **20**, 1561 (2001).
[34]J. H. Jeans, *The Mathematical Theory of Electricity and Magnetism*, 4th ed. (Cambridge University Press, Cambridge, 1920), p. 194.
[35]R. G. Forbes, C. J. Edgcombe, and U. Valdre, Ultramicroscopy **95**, 57 (2003).
[36]A. C. Rose-Innes and E. H. Rhoderick, *Introduction to Superconductivity* (Pergamon Press, Glasgow, 1969), p. 68.
[37]N. M. Jordan, Y. Y. Lau, D. M. French, R. M. Gilgenbach, and P. Pengvanich, J. Appl. Phys. **102**, 033301 (2007).
[38]N. M. Jordan, R. M. Gilgenbach, B. Hoff, and Y. Y. Lau, Rev. Sci. Instrum. **79**, 064705 (2008).